



Corrosion inhibition of mild steel by 6-bromo-1H-imidazo[4,5-b]pyridin-2(3H)-one in 1 M HCl: Experimental and computational study

M. Sikine¹, H. Elmsellem^{2*}, Y. Kandri Rodi¹, H. Steli⁶, A. Aouniti², B. Hammouti²,
Y. Ouzidan¹, F. Ouazzani Chahdi¹, M. Bourass⁵, E. M. Essassi^{3,4}

¹Laboratoire de Chimie Organique Appliquée, Université Sidi Mohamed Ben Abdallah, Faculté des Sciences et Techniques, Route d'Immouzzer, BP 2202 Fes, Morocco

²Laboratoire de chimie analytique appliquée, matériaux et environnement (LC2AME), Faculté des Sciences, B.P. 717, 60000 Oujda, Morocco

³Laboratoire de Chimie Organique Hétérocyclique, URAC 21, Pôle de Compétences Pharmacochimie, Mohammed V University in Rabat, Faculté des Sciences, Av. Ibn Battouta, BP 1014 Rabat, Morocco.

⁴Moroccan Foundation for Advanced Science, Innovation and Research (MASCIR), Rabat Design Center, Rue Mohamed Al Jazouli, Madinat El Irfane, Rabat, Morocco

⁵ECIM/LIMME, Faculty of sciences Dhar El Mahraz, University Sidi Mohamed Ben Abdallah, Fez, Morocco

⁶Laboratoire mécanique & énergétique, Faculté des Sciences, Université Mohammed Premier, Oujda, Maroc

Received 18 Sept 2016, Revised 29 Oct 2016, Accepted 02 Nov 2016

*Corresponding author. E-mail: h.elmsellem@yahoo.fr; Tél: +212670923431/+212600254809

Abstract

The inhibition of mild steel corrosion in 1M HCl of 6-bromo-1H-imidazo[4,5-b]pyridin-2(3H) one (P2) has been studied at various concentrations using mass loss, polarization technique, electrochemical impedance spectroscopy (EIS) and quantum chemical calculations. The mass loss, potentiostatic polarization and EIS results showed that inhibition efficiency (E%) was raised with an increase in concentration of P2 and polarization study also revealed that compound P2 acted as mixed type inhibitor. Adsorption process of the P2 on mild steel surface was found to obey Langmuir adsorption isotherm. Furthermore, calculations from quantum chemical methods were found to be supportive for the results obtained from experimental studies.

Keywords: Imidazopyridine, mild steel, corrosion, inhibition efficiency, EIS, DFT, Fukui function.

1. Introduction

The application of inhibitors is used to reduce the metal dissolution and iron build up in the pickling baths, because the corrosion protection of mild steel is a significant concern among the corrosion scientist and material technologist. Although, mild steel has remarkable economic and substantial applications, its deprived corrosion resistance in acids limits the usage. Acid solutions are essentially used in metal finishing industries, acidizing of oil wells, cleaning of boilers and heat exchangers [1–4].

The most effective and efficient inhibitors are organic compounds containing heteroatom (O, N, S and P) and having p bonds in their structures. The efficiency of an inhibitor is largely dependent on its adsorption on the metal surface. The adsorption of these molecules depend mainly on certain physicochemical properties of the inhibitor molecule such as functional groups, steric factors, aromaticity, electron density at the donor atoms and π orbital character of donating electrons [5,6] and the electronic structure of the molecules [7-8].

Imidazopyridine derivatives are a class of heterocyclic compounds which possess numerous pharmacological properties: anti-inflammatory, anticancer, anti-viral, antiosteoporotic, antiparasitic, antiproliferative, antimicrobial, and anticoccidial [9-13].

The title compound (P2) was obtained in good yield by the condensation of 5-bromo-2,3-diaminopyridine with ethyl chloroformate. The aim of the present study is to evaluate the corrosion inhibition efficiency of mild steel

corrosion in 1 M HCl of 6-bromo-1H-imidazo[4,5-b]pyridin-2(3H)-one (P2) (Figure 1). The structure of the product obtained is determined by spectroscopic and elemental analysis.

Regarding the adsorption of inhibitor on the metal surface, two types of interactions are responsible. One is physical adsorption, which involves electrostatic forces between ionic charges or dipoles of the adsorbed species and the electric charge at the metal/solution interface. The other is chemical adsorption, which involves charge sharing or charge transfer from inhibitor molecules to the metal surface to form coordinate type of bond [14,15].

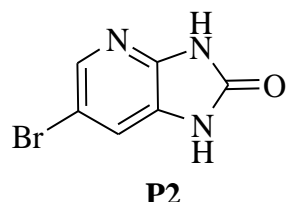


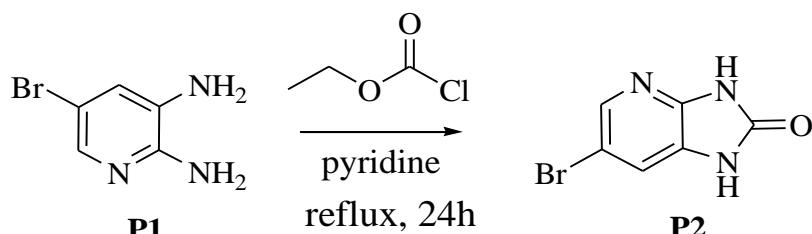
Figure 1. Chemical structure of 6-bromo-1H-imidazo[4,5-b]pyridin-2(3H)-one(**P2**)

Theoretical calculations have been used recently to explain the mechanism of corrosion inhibition, which proved to be a very powerful tool in this direction [16–21]. The geometry of inhibitor molecule in its ground state, nature of its molecular orbitals, HOMO (highest occupied molecular orbital) and LUMO (lowest unoccupied molecular orbital) are directly involved in the corrosion inhibition activity.

2. Experimental

2.1. Synthesis of inhibitor

To a solution of (4g, 0.212 mmole) of 5-bromo-2,3-diaminopyridine in 50 ml of pyridine was added (2.43 ml, 0.255 mmole) of ethyl chloroformate. The magnetic stirring was maintained at 0°C for 15 minutes. Then, the reaction mixture is refluxed for 24 hours. After evaporation of pyridine, the residue obtained was washed with ethanol and then filtered.



Scheme 1. Synthesis of 6-bromo-1H-imidazo[4,5-b]pyridin-2(3H)-one (**P2**).

The analytical and spectroscopic data are conforming to the structure of compound formed: in the spectrum of the proton, we observed two singlets at 11.5 and 11.02 ppm corresponding to the NH protons.

(**P2**): Yield: 65%; M.p>260°C; RMN¹H (DMSO-d6) δ ppm: 11,5(s,1H,NH), 11,02 (s, 1H, NH); 7,93(s,1H,Har) 7,38 (s,1H, Har). RMN¹³C (DMSO-d6) δ ppm: 154,8 (C=O), 144,37 (Cq), 139,97(CH),125,5(Cq), 117,08 (CH), 111,62(Cq).

MS (IE) m/z = 213 [M+. pour ⁷⁹Br], 215 [M+. pour ⁸¹Br]

2.2. Materials and solutions

The steel used in this study is a mild steel with a chemical composition 0.09 wt. % P; 0.38 wt. % Si; 0.01 wt. % Al; 0.05 wt. % Mn; 0.21 wt. % C; 0.05 wt. % S and the remainder iron (Fe).

2.2.1. Preparation of Solutions

The aggressive solutions of 1.0 M HCl were prepared by dilution of analytical grade 37% HCl with distilled water. Inhibitor were dissolved in acid solution at the required concentrations (in mol/l) (volume of inhibitor/volume of HCl), and the solution in the absence of inhibitor was taken as blank for comparison purposes. The test solutions were freshly prepared before each experiment by adding P2 to the corrosive solution. The concentrations of P2 were 10⁻³ to 10⁻⁶ M.

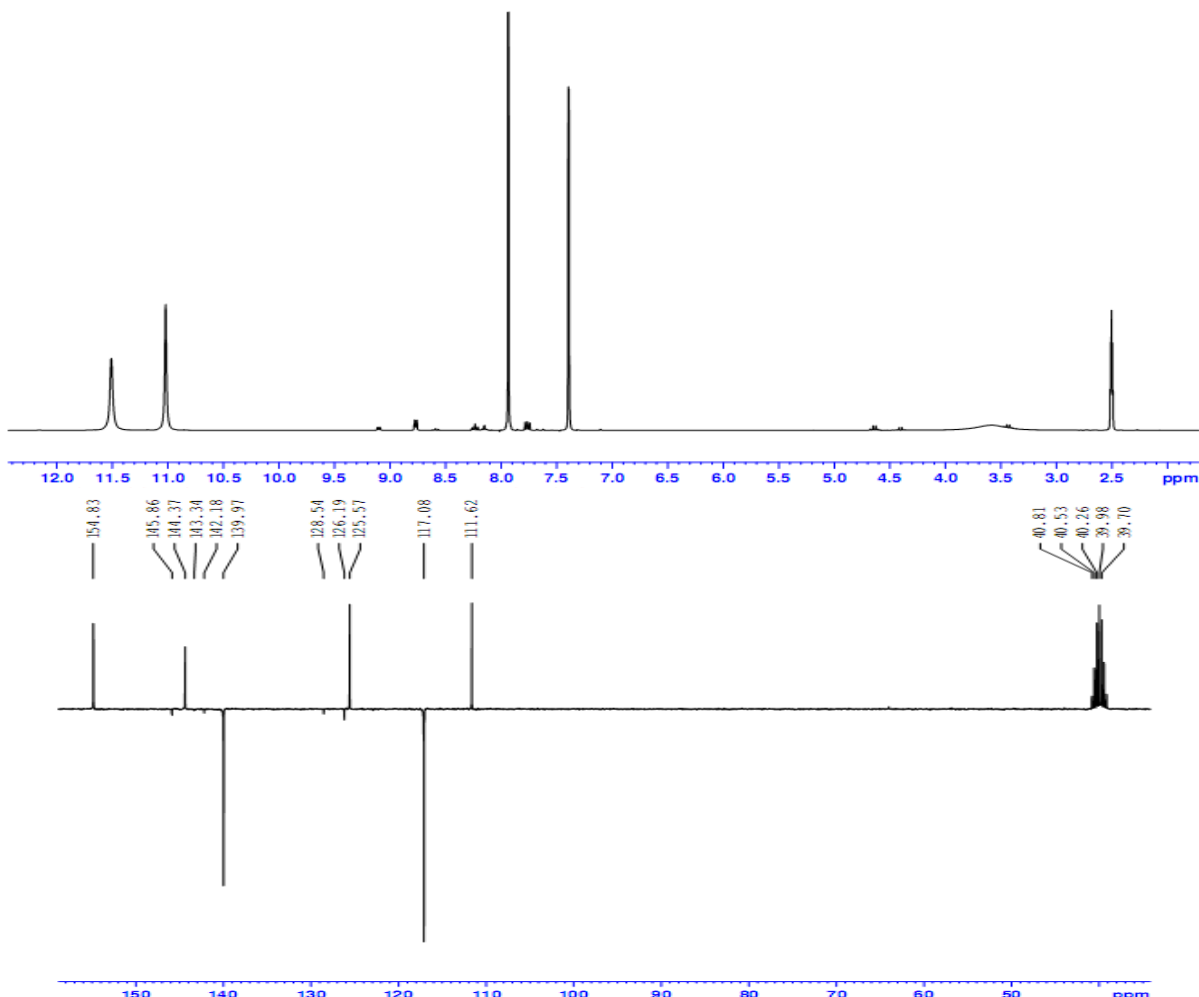


Figure 2: $^{1\text{H}}$ NMR and ^{13}C NMR spectrum of P2

2.2.2. Gravimetric Study

Gravimetric experiments were performed according to the standard methods [22], the carbon steel specimens ($1.5 \text{ cm} \times 1.5 \text{ cm} \times 0.05 \text{ cm}$) were abraded with a series of emery papers SiC (120, 600, and 1200 grades) and then washed with distilled water and acetone. After weighing accurately, the specimens were immersed in a 100 mL of 1.0 M HCl solution with and without addition of different concentrations of inhibitor P2.

All the aggressive acid solutions were open to air. After 6 hours of acid immersion, the specimens were taken out, washed, dried, and weighed accurately. In order to get good reproducibility, all measurements were performed few times and average values were reported.

The average weight loss was obtained. The corrosion rate (v) is calculated using the following equation:

$$v = \frac{W}{St} \quad (1)$$

Where: W is the average weight loss, S the total area, and t is immersion time. With the corrosion rate calculated, the inhibition efficiency (E_w) is determined as follows:

$$E_w \% = \frac{V_0 - V}{V_0} \times 100 \quad (2)$$

Where: v_0 and v are, respectively, the values of corrosion rate with and without inhibitor

2.2.3. Electrochemical Measurements

The electrochemical measurements were carried out using Volta lab (Tacussel - Radiometer PGZ 100) potentiostat controlled by Tacussel corrosion analysis software model (Voltamaster 4) at static condition. The corrosion cell used had three electrodes. The reference electrode was a saturated calomel electrode (SCE). A platinum electrode was used as auxiliary electrode of surface area of 1 cm^2 . The working electrode was carbon steel of the surface 1cm^2 . All potentials given in this study were referred to this reference electrode. The

working electrode was immersed in the test solution for 30 minutes to establish a steady state open circuit potential (E_{ocp}). After measuring the E_{ocp} , the electrochemical measurements were performed. All electrochemical tests have been performed in aerated solutions at 308 K. The EIS experiments were conducted in the frequency range with high limit of 100 kHz and different low limit 0.1 Hz at open circuit potential, with 10 points per decade, at the rest potential, after 30 min of acid immersion, by applying 10 mV ac voltage peak-to-peak. Nyquist plots were made from these experiments. The best semicircle can be fit through the data points in the Nyquist plot using a non-linear least square fit so as to give the intersections with the x-axis.

2.3. Quantum chemical calculations

Quantum chemical calculations are used to correlate experimental data for inhibitors obtained from different techniques (viz., electrochemical and weight loss) and their structural and electronic properties. According to Koopman's theorem [23], E_{HOMO} and E_{LUMO} of the inhibitor molecule are related to the ionization potential (I) and the electron affinity (A), respectively. The ionization potential and the electron affinity are defined as $I = -E_{HOMO}$ and $A = -E_{LUMO}$, respectively. Then absolute electronegativity (χ) and global hardness (η) of the inhibitor molecule are approximated as follows [24]:

$$\chi = \frac{I + A}{2}, \quad \chi = -\frac{1}{2}(E_{HOMO} + E_{LUMO}) \quad (3)$$

$$\eta = \frac{I - A}{2}, \quad \eta = -\frac{1}{2}(E_{HOMO} - E_{LUMO}) \quad (4)$$

Where $I = -E_{HOMO}$ and $A = -E_{LUMO}$ are the ionization potential and electron affinity respectively.

The fraction of transferred electrons ΔN was calculated according to Pearson theory [25]. This parameter evaluates the electronic flow in a reaction of two systems with different electronegativities, in particular case; a metallic surface (Fe) and an inhibitor molecule. ΔN is given as follows:

$$\Delta N = \frac{\chi_{Fe} - \chi_{inh}}{2(\eta_{Fe} + \eta_{inh})} \quad (5)$$

Where χ_{Fe} and χ_{inh} denote the absolute electronegativity of iron atom (Fe) and the inhibitor molecule, respectively; η_{Fe} and η_{inh} denote the absolute hardness of Fe atom and the inhibitor molecule, respectively. In order to apply the eq. 6 in the present study, a theoretical value for the electronegativity of bulk iron was used $\chi_{Fe} = 7$ eV and a global hardness of $\eta_{Fe} = 0$, by assuming that for a metallic bulk $I = A$ because they are softer than the neutral metallic atoms [25].

The electrophilicity has been introduced by Sastri et al. [26], is a descriptor of reactivity that allows a quantitative classification of the global electrophilic nature of a compound within a relative scale. They have proposed the ω as a measure of energy lowering owing to maximal electron flow between donor and acceptor and ω is defined as follows.

$$\omega = \frac{\chi^2}{2\eta} \quad (6)$$

The Softness σ is defined as the inverse of the η [27]

$$\sigma = \frac{1}{\eta} \quad (7)$$

Using left and right derivatives with respect to the number of electrons, electrophilic and nucleophilic Fukui functions for a site k in a molecule can be defined [28]:

$$f_K^+ = P_K(N+1) - P_K(N) \text{ for nucleophilic attack} \quad (8)$$

$$f_K^- = P_K(N) - P_K(N-1) \text{ for electrophilic attack} \quad (9)$$

$$f_K^+ = [P_K(N+1) - P_K(N-1)]/2 \text{ for radical attack} \quad (10)$$

where, $P_k(N)$, $P_k(N+1)$ and $P_k(N-1)$ are the natural populations for the atom k in the neutral, anionic and cationic species respectively.

3. Results and discussion

3.1. Weight loss measurements

The weight loss of mild steel corrosion in 1 M HCl, with and without different concentrations of P2 was determined after 6 h of immersion at 308 K. The obtained results are presented in Table 1.

Table 1. Weight loss data of carbon steel in 1 M HCl without and with different concentrations of P2 at 308 K after 6 h of immersion.

Inhibitor	Concentration (M)	ν (mg.cm ⁻² h ⁻¹)	E_w (%)
1M HCl	--	0.82	--
P2	10⁻⁶	0.29	65
	10⁻⁵	0.23	72
	10⁻⁴	0.11	87
	10⁻³	0.07	91

It has been observed that 10⁻³M of P2 serves as an optimum concentration that exhibit higher efficiency of corrosion inhibition. Since these provide the P2 in excellent corrosion inhibitor. The results indicated that P2 is concentration-independent as inhibition efficiency decrease at highest concentration.

The corrosion rate of mild steel decreased on increasing the inhibitor concentration; This behavior could be attributed to the increase in adsorption of inhibitor at the mild steel/solution interface on increasing its concentration. An increase of inhibitor concentration beyond 10⁻³M resulted in a diminished corrosion protection. This may be due to the withdrawal of adsorbate (inhibitor) back into the bulk solution when the concentration of inhibitor closed to or beyond the critical concentration. The above effect leads to the weakening of metal/inhibitor interactions, resulting in the replacement of inhibitor by water or chloride ions (Cl⁻) with decrease in inhibition efficiency [28]. This may also be due to the inhibitor adsorption at the mild steel surface through non-bonding electron pairs present on nitrogen and oxygen atoms as well as Π -electrons [29]. However, the corrosion inhibition of P2 is essentially due to the presence of electron donor atoms of nitrogen in its molecular structure. So, the electron lone pair on the nitrogen will co-ordinate with the metal atoms of the active sites and will increase adsorption to hence higher inhibition efficiency [30-32].

3.2. Adsorption isotherm and thermodynamic consideration

Corrosion inhibition by organic compounds is mainly due to their ability to adsorb onto a mild steel surface to form a protective film. The establishment of isotherms that describe the adsorption behaviour of corrosion inhibitor is important as they provide clues about the nature of metal-inhibitor interaction. A direct relationship between inhibition efficiency ($E\%$) and the degree of surface coverage (θ) [$E\% / 100 = \theta$] can be assumed for the different concentration of the inhibitor P2. The degree of surface coverage (θ) for the different concentrations of P2 has been evaluated from the weight loss measurements in 1 M HCl at (308 ± 1)K for 6 h of immersion period.

The data were graphically fitted to various adsorption isotherms including Freundlich, Temkin, Flory-Huggins, Bockris- Swinkles, Langmuir and Frumkin isotherms. The correlation coefficient (r) was used to determine the best fit isotherm which was obtained for Langmuir. According to this isotherm, θ is related to the inhibitor concentration by the following equation (12)[33]:

$$\frac{C}{\theta} = \frac{1}{k} + C \quad (11)$$

where θ is the degree of surface coverage, C is the concentration, K_{ads} is the equilibrium constant of adsorption process. K_{ads} is related to the free energy of adsorption ΔG°_{ads} by the equation(13)[34]:

$$\log K_{ads} = -\log C_{H2O} - \left(\frac{\Delta G^\circ_{ads}}{2.303RT} \right) \quad (12)$$

where C_{H2O} is the concentration of water expressed in mol/L (the same as that of inhibitor concentration), R is the molar gas constant (kJ mol⁻¹K⁻¹) and T is the absolute temperature (K).

Figure 3 shows that the plot of C/θ vs. C and linear plots were obtained for the different temperatures indicating that the adsorption of P2 followed Langmuir isotherm. The various adsorption parameters obtained from this isotherm are listed in Table 2.

It is seen from the table that the correlation coefficients are very good and K_{ads} values decrease with an increase in temperature. Large values of K_{ads} mean better inhibition efficiency of the inhibitor, i.e., strong electrical interaction between the double-layer existing at the phase boundary and the adsorbing inhibitor molecules. Small values of K_{ads} , however, reveal that such interactions between adsorbing inhibitor molecules and the metal surface are weaker, indicating that the inhibitor molecules are easily removable by the solvent molecules from the metal surface [35].

Table 2. Some parameters from Langmuir isotherm model for mild steel in 0.01 M HCl.

Inhibitor	Linear correlation (coefficient R)	Slope	K (M^{-1})	ΔG°_{ads} (kJ.mol $^{-1}$)
P2	0.999	1.096	$3.56 \cdot 10^5$	-42.98

These results confirm the suggestion that P2 is physically adsorbed on the metal surface and that the strength of the adsorption decreases with temperature. Although Langmuir plots are linear as depicted by r values (0.999), however, the slopes deviates slightly from the value of unity as expected from ideal Langmuir adsorption equation. This deviation may be explained on the basis of interaction among adsorbed species on the surface of the metal. It has been postulated in the deviation of Langmuir isotherm equation that adsorbed molecules do not interact with one another, but this is not true in the case of large organic molecules (such as P2) having polar atoms or groups which can adsorbed on the cathodic and anodic sites of the metal surface. Such adsorbed species interact by mutual repulsion or attraction. It is also possible that the inhibitor studied can adsorb on the anodic and cathodic sites resulting in deviation from unit gradient. Similar observation has been documented by Solomon et al. [36] and other authors [36, 39].

Calculated free energies ΔG°_{ads} values are given also in Table 2. The negative values of ΔG°_{ads} indicate spontaneous adsorption of P2 onto the mild steel surface [40] and strong interactions between inhibitor molecules and the metal surface [41].

Generally, values of ΔG°_{ads} up to -20 kJ mol $^{-1}$ are consistent with physisorption, while those around -40 kJ mol $^{-1}$ or higher are associated with chemisorption as a result of the sharing or transfer of electrons from organic molecules to the metal surface to form a coordinate bond [42].

The calculated values of ΔG°_{ads} are greater than -40 kJ mol $^{-1}$, indicating that the adsorption mechanism of P2 on mild steel in 1 M HCl solution at the studied 308K may be clearly chemisorption (chemical adsorption of tested compounds on the MS surface) [43].

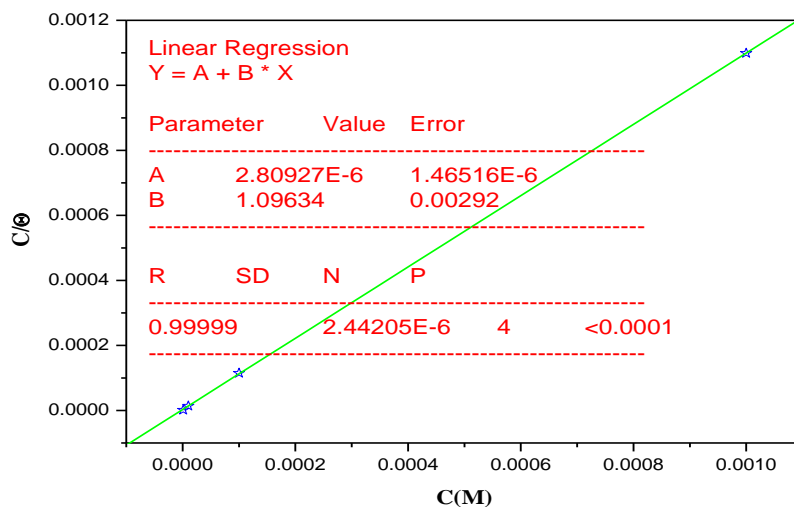
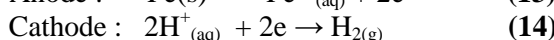


Figure 3. Langmuir adsorption isotherm of P2 on mild steel in 1M HCl at 308K.

3.3. Potentiodynamic polarization

During corrosion of mild steel in HCl, at least one oxidation and one reduction process takes place. Typical reactions involving iron at the electrodes are:



While partial anodic oxidation of the iron results in its dissolution (corrosion), hydrogen gas is liberated at cathode. The compromise or free corrosion potential (E_{corr}) was obtained from the sum total of both cathodic and anodic processes and the corresponding current density (I_{corr}) obtained. Tafel cathodic constants (β_c) were also obtained from the slope of the plots in Figure 4. Some of the P2 parameters determined are shown in Table 3. The I_{corr} values decreased more with increase in inhibitor concentration due to formation of adsorbed protective film.

The corrosion current densities were estimated by Tafel extrapolation of the cathodic curves to the open circuit corrosion potential. The inhibition efficiency was then calculated using the expression:

$$E_P \% = \frac{I_{corr}^\circ - I_{corr}}{I_{corr}^\circ} \times 100 \quad (15)$$

Where I_{corr}° and I_{corr} are uninhibited and inhibited corrosion current densities, respectively.

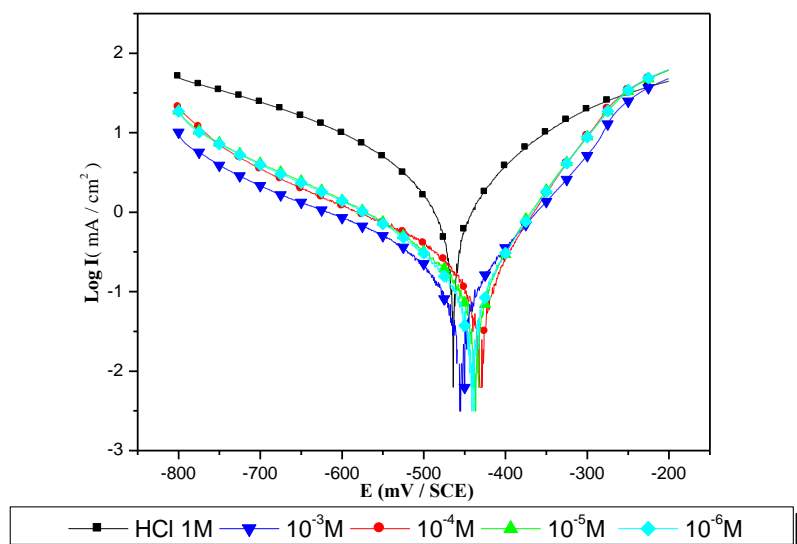


Figure 4. Polarisation curves of mild steel in 1M HCl at different concentrations of P2.

Table 3. Tafel polarization parameters obtained at different concentrations of P2 at 308K.

Inhibitor	Concentration (M)	E_{corr} (mV/SCE)	I_{corr} ($\mu\text{A}/\text{cm}^2$)	$-\beta_c$ (mV dec^{-1})	E_p (%)
HCl	1M	464	1386	184	--
	10^{-6}	436	475	159	66
	10^{-5}	440	311	172	78
	10^{-4}	453	206	163	85
	10^{-3}	445	139	180	90

The values of β_a obtained changes with concentration of inhibitor, showing a definite trend. However, the values of β_c follow no particular trend[44] and the 6-bromo-1H-imidazo[4,5-b]pyridin-2(3H)-one were regarded as mixed type inhibitor with cathodic predominance because the magnitude of the net change was higher in β_c when compared to the free acid solution.

The inhibitor showed a shift in E_{corr} values to more negative values in the inhibited solutions compared to the free acid solution. Usually, cathodic corrosion inhibitors shift the corrosion potential in the negative direction while anodic inhibitors displace the potential in the positive direction [45]. Therefore, the shift to positive E_{corr} values suggests that the inhibitor have dominant influence on the partial anodic reaction. However, the highest shift from that of the free acid (E_{corr}) was less than -85 mV and not sufficient to categorize the inhibitor is cathodic or anodic type. Similar shift in E_{corr} values (less than 85mV) was reported [46, 47] and was regarded as mixed type inhibitors with cathodic predominance. A mixed type inhibitor acts by blocking of some active anodic and cathodic sites of the metal without changing its dissolution or corrosion mechanism. In other words, P2 inhibits both the iron dissolution and hydrogen evolution processes but more actively inhibiting iron oxidation which is anodic reaction.

The calculated inhibition efficiency also increased with increase in concentration of the inhibitor, similar to weight loss.

3.4. Electrochemical impedance spectroscopy

The Electrochemical impedance spectroscopy provides important mechanistic and kinetic information for investigating an electrochemical system. Nyquist impedance plots were obtained for the mild steel electrode at

respective corrosion potentials after 30 min immersion in 1 M HCl in the presence and absence of various concentrations of P2.

The resultant Nyquist plots are shown in Figure 5, respectively. In this case, there was a gradual increase in the diameter of each semicircle of the Nyquist plot as a consequence of the increase in the number of P2 molecules when the concentration was increased from 10^{-6} to 10^{-3} M. This diameter increase clearly showed that the (R_{ct}) values were also increased from 19 to 150 ohms cm^2 at the optimum concentration of 10^{-3} M. Table 4 includes various parameters such as the (R_{ct}), double layer capacitance (C_{dl}) and (E%). The (R_{ct}) values are noted to increase while the (C_{dl}) values gradually decrease from 200 to 19 $\mu\text{F}/\text{cm}^2$ when the inhibitor concentration increases; this can be attributed to the gradual replacement of water molecules by the adsorption of the P2 molecules on the metal surface, decreasing the extent of the dissolution reaction. The higher (R_{ct}) values are generally associated with slower corroding systems [48,49]. The Electrochemical impedance spectroscopy spectra of the investigated inhibitor P2 analyzed using the equivalent circuit, Figure 6, which represents a single charge transfer reaction and fits well with these experimental results. The main parameters deduced from the analysis of the Nyquist diagram are the resistance of charge transfer R_{ct} (diameter of high frequency loop) and the capacity of double layer C_{dl} , which is defined as:

$$C_{dl} = 1/(2\pi f_{max} R_{ct}) \quad (17)$$

Here, f_{max} is the frequency at which the imaginary component of the impedance is maximum- Z_{im} (max). The values of E% were calculated by the equation as follows:

$$E_{EIS} \% = [1 - R_{ct}/R_{inh}] \quad (18)$$

Here, R_{ct} and $R_{ct(inh)}$ are charge-transfer resistance values in the absence and presence of the inhibitor, respectively.

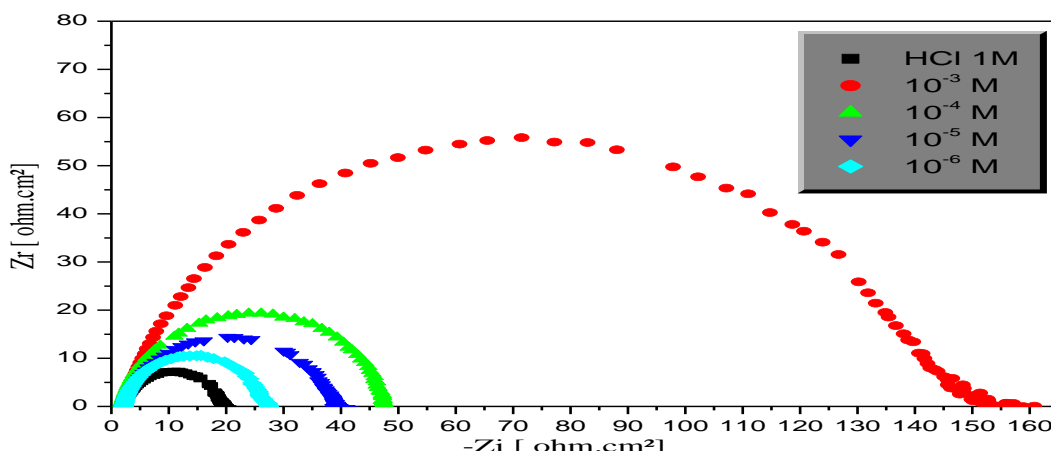


Figure 5. Nyquist diagram for mild steel in 1 M HCl solution in the absence and presence of different concentrations of P2.

Table 4. Electrochemical parameters for mild steel in 1 M HCl at different concentrations of (P2) at 308K.

Inhibitor	Concentration (M)	R_{ct} ($\Omega \text{ cm}^2$)	C_{dl} ($\mu\text{F}/\text{cm}^2$)	E (%)
HCl	1	19	200	--
P2	10^{-6}	26	189	27
	10^{-5}	39	150	51
	10^{-4}	48	79	60
	10^{-3}	150	49	87

The inhibition efficiencies, calculated from Tafel impedance results, show the same trend as those obtained from EIS polarisation and weight loss measurements. Comparison of the efficiencies values (Table 5), obtained

using these three methods, show acceptable agreement. The strong correlation ($R^2 = 0.989$), reveal very good agreement between the obtained data from potentiodynamic polarization curves, electrochemical impedance spectroscopy techniques and weight loss measurement.

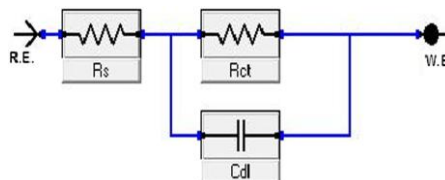


Figure 6. Electrical equivalent circuit model used to fit the impedance results

Table 5. Inhibition efficiency values obtained from weight loss, Tafel polarisation and Ac impedance measurements of carbon steel in 1 M HCl containing various concentrations of P2 at 308K.

P2 Concentration (M)	Inhibition efficiency (E%)		
	Weight loss	Tafel polarisation	Ac impedance
10⁻⁶	65	66	27
10⁻⁵	72	78	51
10⁻⁴	87	85	60
10⁻³	91	90	87

3.5. Computational theoretical studies

The FMOs (HOMO and LUMO) are very important for describing chemical reactivity. The HOMO containing electrons, represents the ability (E_{HOMO}) to donate an electron, whereas, LUMO haven't not electrons, as an electron acceptor represents the ability (E_{LUMO}) to obtain an electron. The energy gap between HOMO and LUMO determines the kinetic stability, chemical reactivity, optical polarizability and chemical hardness–softness of a compound [50]. Firstly, in this study, we calculated the HOMO and LUMO orbital energies by using B3LYP method with 6-31G which is implemented in Gaussian 09 package [51-52]. All other calculations were performed using the results with some assumptions. The higher values of E_{HOMO} indicate an increase for the electron donor and this means a better inhibitory activity with increasing adsorption of the inhibitor on a metal surface, whereas E_{LUMO} indicates the ability to accept electron of the molecule. The adsorption ability of the inhibitor to the metal surface increases with increasing of E_{HOMO} and decreasing of E_{LUMO} . The HOMO and LUMO orbital energies of the P2 inhibitors were performed and were shown in Table 6 and Figure 7. High ionization energy (> 6 eV) indicates high stability of P2 inhibitor [53], the number of electrons transferred (ΔN), dipole moment, Ionization potential, electron affinity, electronegativity, hardness, Softness and total energy were also calculated and tabulated in Table 6.

Table 6: Quantum chemical parameters for P2 obtained in gas and aqueous phase with the DFT at the B3LYP/6-31G level.

Parameters	Gas phase	Aqueous phase
Total Energy TE (eV)	-82645.8	-82646.4
E_{HOMO} (eV)	-10.3379	-9.8318
E_{LUMO} (eV)	-3.0775	-1.9071
Gap ΔE (eV)	7.2604	7.9246
Dipole moment μ (Debye)	2.6382	3.5424
Ionization potential I (eV)	10.3379	9.8318
Electron affinity A	3.0775	1.9071
Electronegativity χ	6.7077	5.8695
Hardness η	3.6302	3.9623
Electrophilicity index ω	6.1970	4.3473
Softness σ	0.2755	0.2524
Fractions of electron transferred ΔN	0.0403	0.1427

The value of ΔN (number of electrons transferred) show that the inhibition efficiency resulting from electron donation agrees with Lukovit's study [54]. If $\Delta N < 3.6$, the inhibition efficiency increases by increasing electron donation ability of these inhibitors to donate electrons to the metal surface [55-56].

Pertinent valence and dihedral angles, in degree, of the studied inhibitor calculated at B3LYP/6-31G(d,p) in gas and aqueous phases are given in the table 6.

Table 7 displays the most relevant values of the natural population ($P(N)$, $P(N-1)$ and $P(N+1)$) with the corresponding values of the Fukui functions (f_k^+ , f_k^- and f_k^0) of the studied inhibitors. The calculated values of the f_k^+ for inhibitors are mostly localized on the imidazopyridine ring, namely C₂, C₅, C₆, N₁₂, N₁₃, O₁₄ and Br₁₅, indicating that the imidazopyridine ring will probably be the favorite site for nucleophilic attacks.

Table 7: Pertinent natural populations and Fukui functions of P2 calculated at B3LYP/6-31G in gas (G) and aqueous phases.

Atom k	Phase	P(N)	P(N-1)	P(N+1)	f_k^-	f_k^+	f_k^0
C_2	G	5,56923	5,67715	5,52746	0,1079	0,0418	0,0748
	A	5,56375	5,68526	5,52746	0,1215	0,0363	0,0789
C_5	G	6,23269	6,3948	6,23743	0,1621	-0,0047	0,0787
	A	6,21411	6,38763	6,23743	0,1735	-0,0233	0,0751
C_6	G	5,04336	5,05689	5,17641	0,0135	-0,1331	-0,0598
	A	5,0307	5,05349	5,17641	0,0228	-0,1457	-0,0615
N_{12}	G	7,76422	7,76483	7,64059	0,0006	0,1236	0,0621
	A	7,76385	7,77192	7,64059	0,0081	0,1233	0,0657
N_{13}	G	7,49989	7,72179	7,48864	0,2219	0,0112	0,1166
	A	7,53485	7,7816	7,48864	0,2468	0,0462	0,1465
O_{14}	G	8,72129	8,80831	8,35309	0,0870	0,3682	0,2276
	A	8,78256	8,83596	8,35309	0,0534	0,4295	0,2414
Br_{15}	G	34,91679	35,04284	34,79295	0,1260	0,1238	0,1249
	A	34,92436	35,01212	34,79295	0,0878	0,1314	0,1096

The geometry of P2 in gas and aqueous phase (Figure 7) were fully optimized using DFT based on Beck's three parameter exchange functional and Lee–Yang–Parr nonlocal correlation functional (B3LYP) [57-58] and the 6–31G. The optimized structure shows that the molecule P2 has a non-planar structure. The HOMO and LUMO electrons density distributions of **P2** are given in Table 8.

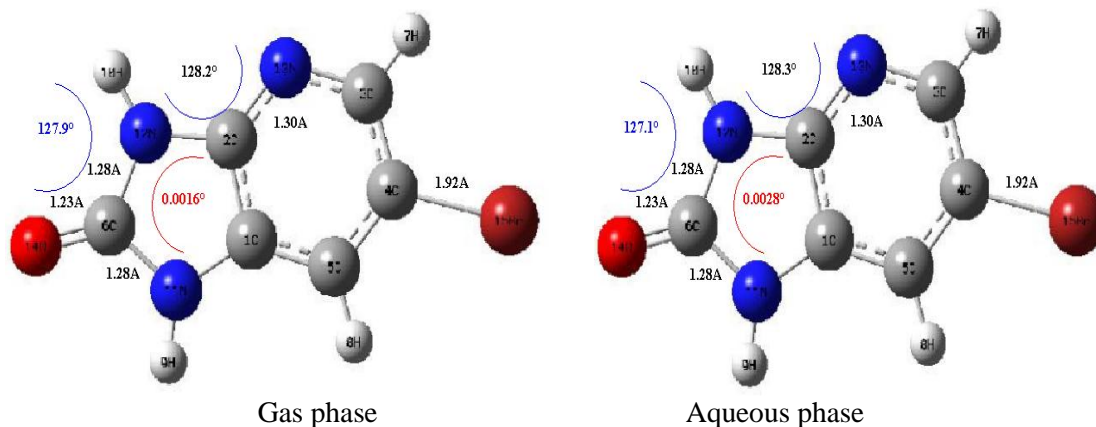
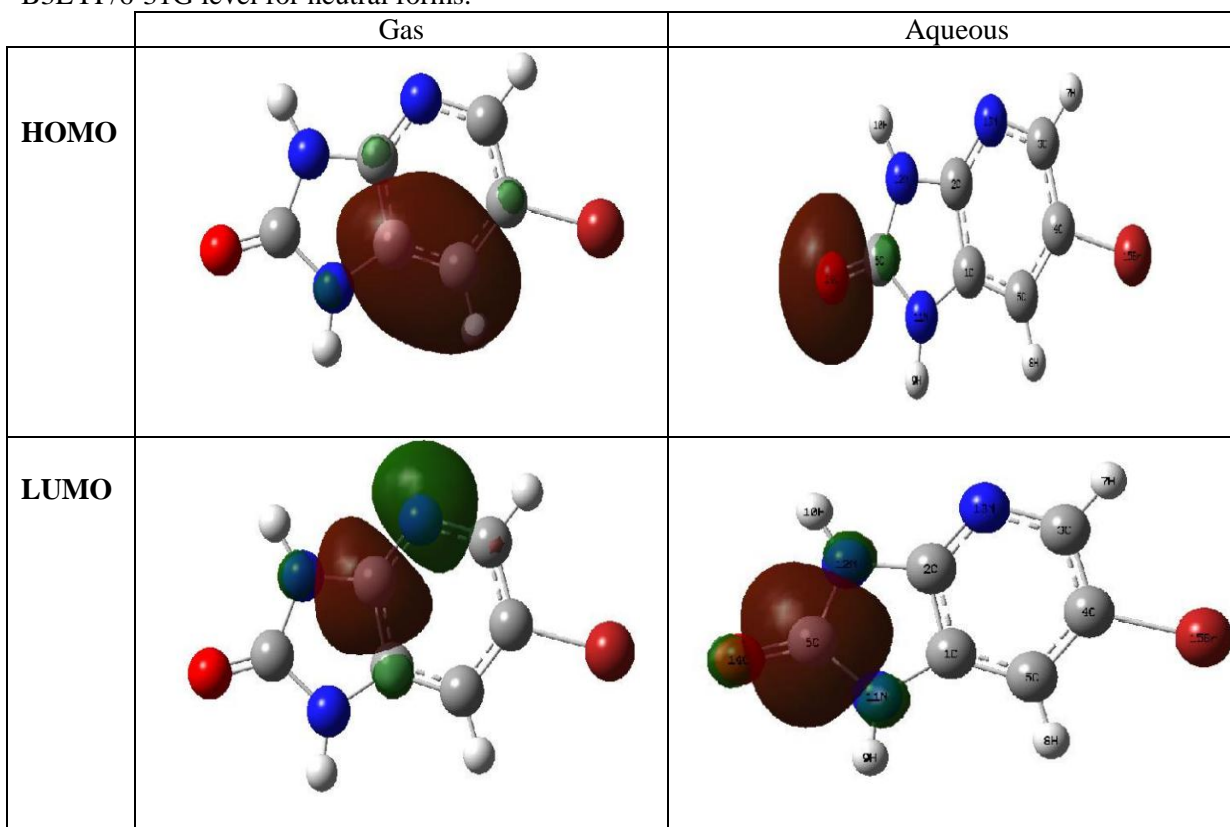


Fig. 7: Optimized molecular structures and selected dihedral angles (red), angles (blue) and bond lengths (black) of the studied inhibitors calculated in gaseous and aqueous phases using the DFT at the B3LYP/6-31G level.

As we know, frontier orbital theory is useful in predicting the adsorption centres of the inhibitors responsible for the interaction with surface metal atoms. Table 8 shows the HOMO and LUMO orbital contributions for the neutral studied inhibitor. The HOMO densities were concentrated on isatine ring.

Table 8. The HOMO and the LUMO electrons density distributions of P2 in gas and aqueous phase computed at B3LYP/6-31G level for neutral forms.

- ✓ The obtained results show that P2 acts as mixed-type inhibitor of corrosion inhibition of mild steel in 1 M HCl.
- ✓ EIS measurement results indicate that the resistance of the mild steel electrode increases greatly and its capacitance decreases by increasing the inhibitor concentration.
- ✓ Reasonably good agreement was observed between the obtained data from potentiodynamic polarization curves and electrochemical impedance spectroscopy techniques.
- ✓ Quantum chemical calculations using DFT reveal that the adsorption of P2 on mild steel would takes place through the biheterocyclic system. The simultaneous adsorption of the three functional groups forces the inhibitor molecule to be horizontally oriented at the metal surface.
- ✓ The introduction of P2 into 1 M HCl solution results in the formation of a protective film on the mild steel surface, which may contain the complex of P2-Fe²⁺, and effectively protects steel from corrosion.

Reference

1. El-Taib H.F., Haryama S., *Corros. Sci.*, 20 (1980) 887–896.
2. Al-Abdullah M.M., Abu-Orabi S.T., *Corrosion*. 22 (1991) 150–154.
3. Abdennaby A.M.S., Abdulhadi A.I., Abu-Orabi S.T., Saricimen H., *Corros. Sci.* 38 (1996) 1791–1800.
4. Mernari B., Elattari H., Traisnel M., Bentiss F., Lagrenée M., *Corros. Sci.* 40 (1998) 391–399.
5. Lukovits I., Kalman E., Palinkas G., *Corrosion*. 51 (1995) 201–205.
6. Bentiss F., Lagrenée M., Traisnel M., Mernari B., El Attari H., *J. Heterocyclic Chem.* 36 (1999) 149–152.
7. Bentiss F., Lagrenée M., Traisnel M., Hornez J.C., *Corros. Sci.* 41 (1999) 789.
8. Chetouani A., Hammouti B., Medjahed K., Mansri A., *Der Pharma Chemica*, 3 (2011) 307–316.
9. Dymin'ska L., *Bioorganic & Medicinal Chemistry*. 23 (2015) 6087–6099.
10. Seung-Chul L., Hyun Tae K., Choul-Hong P., Do Young L., Ho-Jin C., Sunggu R., Young-Ger S., *Bioorganic & Medicinal Chemistry Letters*. 22 (2012) 4221–4224.
11. Sakthivel M., Yu-Wei C., Matthew A., Alexus D., Marisha M., Valerie A., Odero-M., Khan S. A., William G., *Cancer Letters*. 353 (2014) 59–67.
12. Al-Tel T., Al-Qawasmeh R., Zaarour R., *European Journal of Medicinal Chemistry*. 46 (2011) 1874–1881.
13. Scribner A., Dennis R., Hong J., Lee S., McIntyre D., Perrey D., Feng D., Fisher M., Wyvratt M., Leavitt P., Liberator P., Gurnett A., Brown C., Mathew J., Thompson D., Schmatz D., Biftu T., *European Journal of Medicinal Chemistry*. 42 (2007) 1334–1357.
14. Avci G., *Colloids Surf. A*. 317 (2008) 730–736.
15. Noor E.A., Al-Moubaraki A.H., Mater. Chem. Phys. 110 (2008) 145–154.
16. Gece G., Bilgic S., *Corros. Sci.* 52 (2010) 3304–3308.
17. Radilla J., Negron-Silva G.E., Palomar-Pardave M., Romero-Romo M., Galvan M., *Electrochim. Acta*. 112(2013)577–586.
18. Arslan T., Kandemirli F., Ebenso E.E., Love I., Alemu H., *Corros. Sci.*, 51 (2009) 35–47.
19. Herrag L., Hammouti H., Elkadiri S., Aouniti A., Jama C., Vezin H., Bentiss F., *Corros. Sci.* 52 (2010) 3042–3051.
20. Zarrok H., Oudda H., B. Zarrouk A., Salghi R., Hammouti B., Bouachrine M., *Der Pharm. Chem.* 3 (2011) 576–590.
21. Bouklah M., Hammouti, A. Aouniti, Benkaddour M., Bouyanzer A., *Appl. Surf. Sci.* 252 (2006) 6236–6242.
22. Essaghouani A. L., Elmsellem H., Ellouz M., El Hafi M., Boulhaoua M., Sebbar N. K., Essassi E. M., Bouabdellaoui M., Aouniti A. and Hammouti B., *Der Pharma Chemica*. 8(2) (2016) 297-305.
23. Pearson R.G., Inorg. Chem. 27 (1988) 734–740.
24. Sastri V.S., Perumareddi J.R., *Corrosion*. 53 (1997) 617–622.
25. Pearson R.G., *Inorg. Chem.* 27 (1988) 734.
26. Sastri, V. and Perumareddi S., *J.R. Corrosion*, 53 (1997) 671.
27. Udhayakala P., Rajendiran T. V., and Gunasekaran S., *Journal of Chemical, Biological and Physical Sciences A*. 2(3) (2012) 1151-1165.
28. Roy R.K., Pal S., Hirao K., *J. Chem. Phys.* 110 (1999) 8236.
29. Hjouji M. Y., Djedid M., Elmsellem H., Kandri Rodi Y., Benalia M., Steli H., Ouzidan Y., Ouazzani Chahdi F., Essassi E. M., Hammouti B., *Der Pharma Chemica*. 8(4) (2016) 85-95.

30. Elmsellem H., Bendaha H., Aouniti A., Chetouani A., Mimouni M., Bouyanzer A., *Mor. J. Chem.* 2 (1) (2014) 1-9.
31. Elmsellem H., Elyoussi A., Sebbar N. K., Dafali A., Cherrak K., Steli H., Essassi E. M., Aouniti A. and Hammouti B., *Maghr. J. Pure & Appl. Sci.* 1 (2015) 1-10.
32. Elmsellem H., Aouniti A., Khoutoul M., Chetouani A., Hammouti B., Benchat N., Touzani R. and Elazzouzi M., *J. Chem. Pharm. Res.* 6 (2014) 1216.
33. Chakib I., Elmsellem H., Sebbar N. K., Lahmadi S., Nadeem A., Essassi E. M., Ouzidan Y., Abdel-Rahman I., Bentiss F., Hammouti B., *J. Mater. Environ. Sci.* 7(6) (2016) 1866-1881.
34. Elmsellem H., Harit T., Aouniti A., Malek F., Riahi A., Chetouani A., Hammouti B., *Protection of Metals and Physical Chemistry of Surfaces*. 51(5) (2015) 873.
35. Amin M.A., Mohsen Q., Hazzazi O.A., *Mater. Chem. Phys.* 114 (2009) 908.
36. Amin M.A., Abd El Rehim S.S., El-Naggar M.M., Abdel-Fatah H.T.M., *J. Mater. Sci.* 44 (2009) 6258.
- 37- Elmsellem H., Elyoussi A., Steli H., Sebbar N. K., Essassi E. M., Dahmani M., El Ouadi Y., Aouniti A., El Mahi B., Hammouti B., *Der Pharma Chemica*. 8(1) (2016) 248.
38. Migahed M.A., Mohammed H.M., Al-Sabagh A.M., *Mater. Chem. Phys.* 80 (2003) 169.
39. Solomon M.M., Umuren S.A., Udosoro I.I., Udoeh A.P., *Corros. Sci.* 52(4) (2010) 1317.
40. Elmsellem H., Basbas N., Chetouani A., Aouniti A., Radi S., Messali M., Hammouti B., *Portugaliae. Electrochimica. Acta*. 2 (2014) 77.
41. Tang I., Li X., Lin I., Mu G., Liu G., *Mater. Chem. Phys.* 97 (2006) 301.
42. Sibel Z., Dogan P., Yazici B., *Corros. Rev.* 23 (2005) 217.
43. Elmsellem H., Nacer H., Halaimia F., Aouniti A., Lakehal I., Chetouani A., Al-Deyab S. S., Warad I., Touzani R., Hammouti B., *Int. J. Electrochem. Sci.* 9(2014) 5328.
44. Anupama K.K., Ramya K., Shainy K.M., Joseph A., *Chem. Phys.* 167 (2015) 28-41.
45. Elmsellem H., Aouniti A., Youssoufi M.H., Bendaha H., Ben hadda T., Chetouani A., Warad I., Hammouti B., *Phys. Chem. News.* 70 (2013) 84.
46. Fouda A.S., Shalabi S.K., Elewady G.Y., Merayyed H.F., *Int. J. Electrochem. Sci.* 9 (2014) 7038-7058.
47. Elmsellem H., Aouniti A., Toubi Y., Steli H., Elazzouzi M., Radi S., Elmahi B., El Ouadi Y., Chetouani A., Hammouti B., *Der Pharma Chemica*. 7(7) (2015) 353-364.
48. Hsu C., Mansfeld F., *Corrosion*. 57 (2001) 747-748
49. Ellouz M., Elmsellem H., Sebbar N. K., Steli H., Al Mamari K., Nadeem A., Ouzidan Y., Essassi E. M., Abdel-Rahaman I., Hristov P., *J. Mater. Environ. Sci.* 7(7) (2016) 2482-2497.
50. Govindarajan M., Karabacak M., *Spectrochim Acta Part A Mol Biomol Spectrosc*, 85 (2012) 251-60.
51. Becke A.D., *J. Chem. Phys.* 98 (1993) 1372.
52. Filali Baba Y., Elmsellem H., Kandri Rodi Y., Steli H., AD C., Ouzidan Y., Ouazzani Chahdi F., Sebbar N. K., Essassi E. M., and Hammouti B., *Der Pharma Chemica*, 8(4)(2016) 159-169.
53. Elmsellem H., Karrouchi K., Aouniti A., Hammouti B., Radi S., Taoufik J., Ansar M., Dahmani M., Steli H. and El Mahi B., *Der Pharma Chemica*, 7(10) (2015) 237-245.
54. Lukovits I., Kalman E., Zucchi F., *Corrosion*, 57 (2001) 3-7.
55. Sikine M., Kandri Rodi Y., Elmsellem H., Krim O., Steli H., Ouzidan Y., Kandri Rodi A., Ouazzani Chahdi F., Sebbar N. K., Essassi E. M., *J. Mater. Environ. Sci.* 7 (4) (2016) 1386-1395.
56. Elmsellem H., Elyoussi A., Steli H., Sebbar N. K., Essassi E. M., Dahmani M., El Ouadi Y., Aouniti A., El Mahi B., Hammouti B., *Der. Pharma. Chemica*. 8(1)(2016) 248-256.
57. Lee C., Yang W., Parr R.G., *Phys. Rev.* B37(1988) 785.
58. Al Mamari K., Elmsellem H., Sebbar N.K., Elyoussi A., Steli H., Ellouz M., Y. Ouzidan Y., Nadeem A., Essassi E.M., El-Hajjaji F., *J. Mater. Environ. Sci.* 7(9) (2016) 3286-3299.
59. K. Ramji, D.R. Cairns, S. Rajeswari, *Appl. Surf. Sci.* 254 (2008) 4483.
60. Obot I.B., Obi-Egbedi N.O., *Corros. Sci.* 52 (2010) 198.
61. Ashassi-Sorkhabi H., Nabavi-Amri S.A., *Acta Chim. Slov.* 47 (2000) 512.